LAWRENCE
LIVERMORE
NATIONAL
LABORATORY

LLNL-JRNL-575292

Probing matter at extreme Gbar pressures at the NIF

A. Kritcher, D. Swift, R. W. Falcone, T. Doeppner, S. Felker, G. Collins, O. L. Landen, H. J. Lee, J. Hawreliak, S. H. Glenzer, J. Hammer, C. Keane

August 20, 2012

High Energy Density Physics

Disclaimer

This document was prepared as an account of work sponsored by an agency of the United States government. Neither the United States government nor Lawrence Livermore National Security, LLC, nor any of their employees makes any warranty, expressed or implied, or assumes any legal liability or responsibility for the accuracy, completeness, or usefulness of any information, apparatus, product, or process disclosed, or represents that its use would not infringe privately owned rights. Reference herein to any specific commercial product, process, or service by trade name, trademark, manufacturer, or otherwise does not necessarily constitute or imply its endorsement, recommendation, or favoring by the United States government or Lawrence Livermore National Security, LLC. The views and opinions of authors expressed herein do not necessarily state or reflect those of the United States government or Lawrence Livermore National Security, LLC, and shall not be used for advertising or product endorsement purposes.

Probing matter at Gbar pressures at the NIF

A. L. Kritcher[1], T. Döppner[1], D. Swift[1], J. Hawreliak[1], S. H. Glenzer[3], G. Collins[1], S. Felker[1], O. L. Landen[1], H. J. Lee[3], S. Rothman[4], D. Chapman[4], C. Thomas[1], O. Jones[1], J. Hammer[1], C. Keane[1], and R. W. Falcone[2]
[1]*L-493, Lawrence Livermore National Laboratory, Livermore, CA, USA*
[2]*Department of Physics, University of California Berkeley, Berkeley, CA, USA*
[3]*SLAC Accelerator National Laboratory, Menlo Park, CA, USA and*
[4]*Atomic Weapons Establishment, Reading, United Kingdom*
(Dated: August 19, 2013)

We describe a platform to measure the material properties, specifically the equation of state and electron temperature, at pressures of 100 Mbar to a Gbar at the National Ignition Facility (NIF). In these experiments we will launch spherically convergent shock waves into solid CH, CD, or diamond samples using a hohlraum radiation drive, in an indirect drive laser geometry. X-ray radiography will be applied to measure the shock speed and infer the mass density profile, enabling determining of the material pressure and Hugoniot equation of state. X-ray scattering will be applied to measure the electron temperature through probing of the electron velocity distribution via Doppler broadening.

PACS numbers: 52.25.Os, 52.35.Fp, 52.50.Jm
Keywords: X-ray Scattering, X-ray Radiography, Gbar, Thomson Scattering, Compton Scattering, Shock Compression

INTRODUCTION

Matter at extreme pressures, of 100 Mbar to > Gbar, occurs widely in astrophysical objects such as gas-giant planets [1, 2] or highly evolved stars [3]. Laboratory measurements of the Equation of State (EOS) of matter at high energy density is of great importance in understanding the structure and evolution of these objects and for accurate modeling of matter at extreme conditions. For example, at Gbar pressures atomic shell effects [4] may come into play which can change the predicted compressibility at given pressure due to pressure and temperature ionization. Recent advances in experimental capabilities to produce high-energy-density plasmas (HEDP) using high-energy lasers enables the creation of these astrophysically relevant conditions in the laboratory (e. g.> 500 g/cc (>10^{26} e-/cc), > 10 keV) at the National Ignition Facility (NIF) [5]. Here, we propose to create these extreme material conditions at the NIF in a convergent shock geometry and probe quantum shell effects through measurement of the equation of state and electron temperature.

In addition, benchmarking state-of-the-art computational dense matter models in this regime is also of central interest for fusion energy experiments that are designed to assemble fusion fuel to the highest densities ever achieved in the laboratory environment [6, 7]. Specifically, we propose a platform to probe the EOS of CH at pressures in the range of 100-1000 Mbar, which has been widely used as the ablator material in fusion experiments at the NIF. Previous experiments to measure the EOS of polystyrene have benchmarked models at pressures of up to 40 Mbar at the Nova laser facility [8], up to 27 Mbar at the GEKKO/HIPER laser facility [9], and up to 1-10 Mbar in high precision experiments at the Omega laser facility [10]. These experiments use planar driven shock waves to drive the samples to high pressures and impedance-matching to a quartz standard to determine the principle shock Hugoniot [11, 12]. However, at pressures >100 Mbar this method can no longer be used, as the quartz standard becomes reflective and data can no longer be obtained [13]. In addition reaching these pressures in a planar geometry is currently not feasible for the mm scale sample sizes required to employ other diagnostics such as x-ray radiography.

In this work we present a platform to study the EOS of material compressed to Gbar pressures in a spherically convergent shock wave geometry, using x-ray radiography and x-ray Thomson scattering. Current experiments on the NIF that reach pressures of >100 Mbar in the fuel layer of converging ignition capsules have measured the velocity and shell thickness via streaked radiography [14, 15]. However, in this platform the EOS of the ablator material cannot be constrained due to thin shell effects, uncertainties in determining the mass density profile, and uncertainties in the opacity. We will drive a strong convergent shock wave through solid spherical targets in an indirectly driven laser hohlraum geometry at the NIF, which will provide a known density inside of the shocked region, greatly improving the mass density unfold analysis [16]. A Ge doped ablator on the exterior of the target will provide a total mass density fiducial for the radiographic unfold and will also be used to mitigate preheat due to Au M-band emission from the hohlraum. By measuring the mass density profile and shock speed from the radiographic signal, we can infer the pressure in the shocked region using the Hugoniot relations.

We will simultaneously measure the density weighted electron temperature using x-ray Thomson scattering [17–24]. The ionization state of the material can also be inferred using x-ray scattering which will enabling the study of shell ionization effects at Gbar pressures. In the

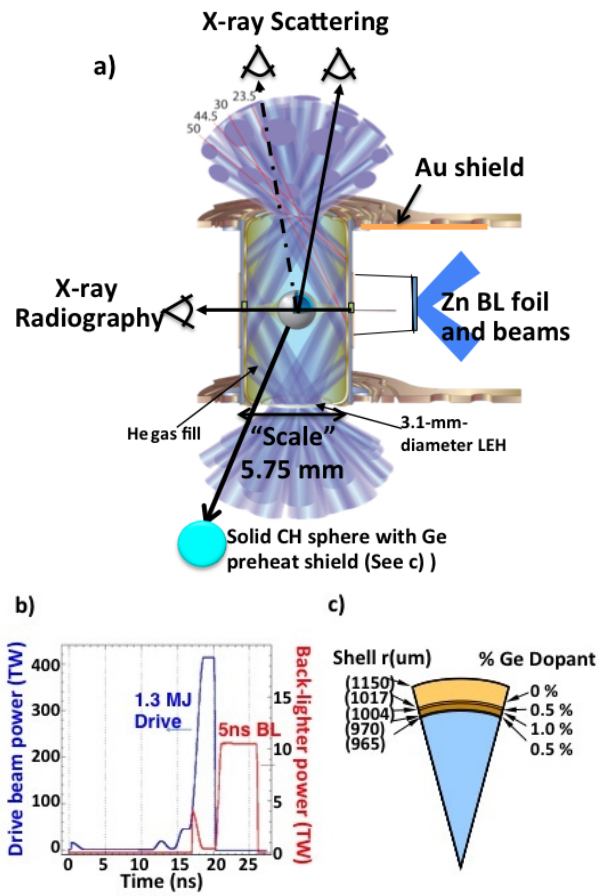

FIG. 1: a) Schematic of the experimental setup. Here solid targets of CH or CD are shock compressed using a hohlraum radiation source. The plasma will be probed with x-ray radiography in the equatorial DIM and x-ray scattering in the polar DIM. b) Power profiles vs time of the laser drive and backlighter beams. c) Wedged cross-section of the solid CH target with a Ge doped CH ablator. Shown on the left hand side are the radii of the layers, and shown on the right hand side are the percent dopant of the Ge layers.

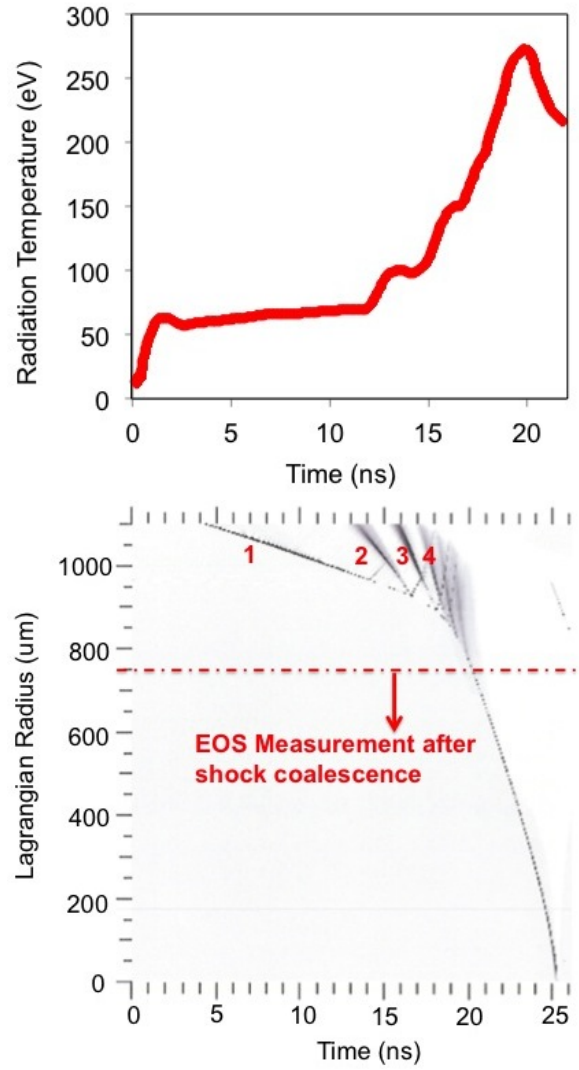

FIG. 2: (top) Radiation temperature as a function of time, derived from integrated Hohlraum simulations. (bottom) Normalized pressure gradients with respect to space and time, showing shock evolution, with the first second, and third shocks listed. The EOS measurement takes place after the four shocks have coalesced into one single strong shock.

following sections, we will present planned experiments at the NIF to employ these techniques, under an accepted NIF basic science shot-time allocation.

These experiments will make use of the extensive shock timing and cross-beam energy transfer tuning effort of the National Ignition Campaign (NIC) [25–32] to ensure adequate drive symmetry required for the radiographic unfold. In addition, we will employ an existing technique that is used to measure streaked radiographs at the NIF from material compressed to >10 g/cc [33]. To field x-ray Thomson scattering at NIF we have designed and fabricated a new spectrometer that can be operated with the NIF x-ray framing cameras [34], enabling gated detection of the scattered signal. This development builds on previous successful experiments at the Omega laser facility [18] where high-quality scattering from imploding CH and Be spheres enabled measurement of the electron temperature and density of the highly compressed capsules (about 6 and 13 times solid density). We further employ this technique to probe compressions of 4.5 to >15 (behind the shock front) times solid density in solid spheres at the NIF.

EXPERIMENTAL PLATFORM

A schematic of the experimental configuration is shown Fig. 1. In these experiments, solid targets will be compressed and heated in an indirect drive laser geometry

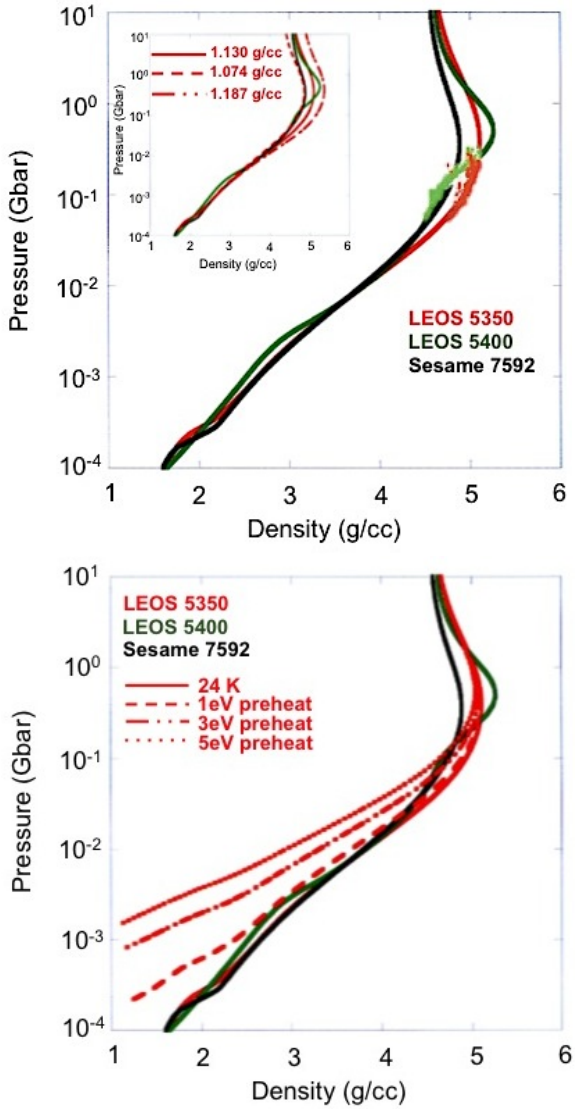

FIG. 3: (top) Principle shock Hugoniots for glow-discharge polymer equations of states LEOS 5350 and LEOS 5400, and a polystyerene equation of state Sesame 7592. The red and green points plotted on the LEOS 5350 and 5400 curves are extracted from the rad-hydro simulations that use these choices of EOS, respectively, showing that after shock coalescence we follow the principle hugoniot. (top inset) Sensitivity of EOS LEOS 5350 to uncertainty in initial target density. (bottom) Sensitivity of EOS LEOS 5350 to initial temperature, or preheat, from Au M-band x-rays or hot electrons.

using 184 laser beams incident on an Au hohlraum. In the first experiments the targets will consist of solid CH or CD spheres 1.9 mm in diameter covered by a 185 μm thick CH ablator with a graded Ge dopant, see Fig. 1 c). Target fabrication and coating of the CH spheres will be done at General Atomics (GA). The graded doped CH ablator is fabricated via the same method as NIC ablators where the CH material is a glow-discharge polymer (GDP). The Ge dopant is used to mitigate preheat induced by Au M-shell emission from the gold hohlraum. The solid spheres are constructed in the same method as NIC mandrels for ICF capsules. This material is poly(alpha-methylstyrene) or PAMS. In the first experiments we will shoot a cryogenically cooled hohlraum and target, to be consistent with previous NIC experiments. For the purposes of this study, the initial equilibrium density of 1.13 g/cc was taken from polystyrene EOS Sesame 7592 at 24K and zero pressure.

In the first experiments we will use a standard NIC scale 5.75 mm hohlraum (diameter =5.75 mm and height=9.42 mm) with a 0.96 mg/cc He gas fill and 3.375 mm diameter laser entrance hole. A 5 or 15 μm thick zinc backlighter foil is positioned six mm from the target chamber center, and two diagnostic slits in the hohlraum (170 μm x 2.4 mm) enable transmission of the radiographic backlighter through the hohlraum walls. The hohlraum drive energy will be delivered by 184, 351nm laser beams with the NIC Rev5 pulse shape, see Fig. 1 b). The total laser drive energy and power incident on the hohlraum walls will be about 415 TW and ∼1.3 MJ, respectively. These drive conditions will result in a predicted hohlraum radiation temperature of about 270 eV, see Fig.2.

To characterize the compressed spheres with x-ray scattering a laser-produced zinc He-α x-ray source (8.99 keV) delayed in time from the drive beams will be scattered from the targets at either 84.5°t in the polar direction, accessing the non-collective regime of the plasma at this probe energy and scattering angle. The same x-ray source will be used for radiography by an x-ray streak camera in the equatorial DIM. The source will be produced using eight additional shaped laser beams with a peak laser power of about 10.6 TW for 5 ns, see Fig.1 b). An additional gold shield, 50μm thick, with a 15μm thick coating of CH, will be used to ensure that the x-ray scattering spectrometer in the Polar DIM detects only scattered x-rays from the target and not the backlighter photons.

RADIATION HYDRODYNAMIC SIMULATIONS

In this section we present radiation hydrodynamics simulations of the predicted plasma conditions for this platform using the code HYDRA [35]. These simulations are capsule-only simulations that use a frequency dependent radiation drive that surrounds the capsule. This drive is derived from integrated Hohlraum simulations which includes the non-Planckian behavior of the drive. Integrated simulations enable modeling of laser beam propagation and absorption using the exact laser beam power time histories and pointings for a specific target configuration. However, known losses due to laser-plasma interactions are not included, and have been his-

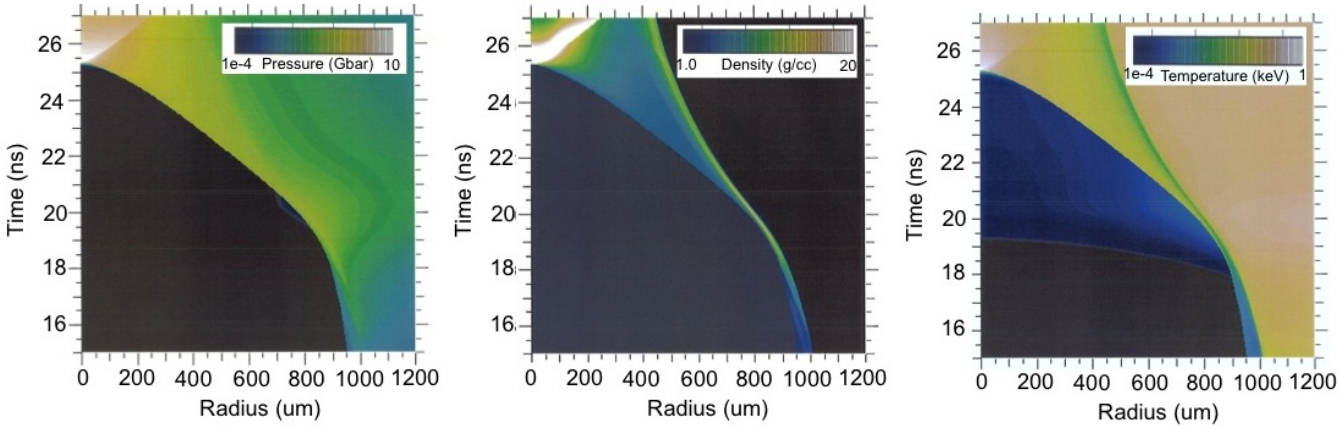

FIG. 4: Contour plots of the pressure, density, and ion temperature as a function of radius and time for simulations using equation of state LEOS 5350. Here, the pressure color contour is plotted logarithmically from 1×10^{-4} to 10 (Gbar), the density color contour is plotted linearly from 1 to 20 (g/cc), and the temperature color contour is plotted logarithmically from 1×10^{-4} to 1 (keV). The preheat from Au M-band absorption past the Ge preheat shield, as seen in the temperature contour plot, is <0.3 eV.

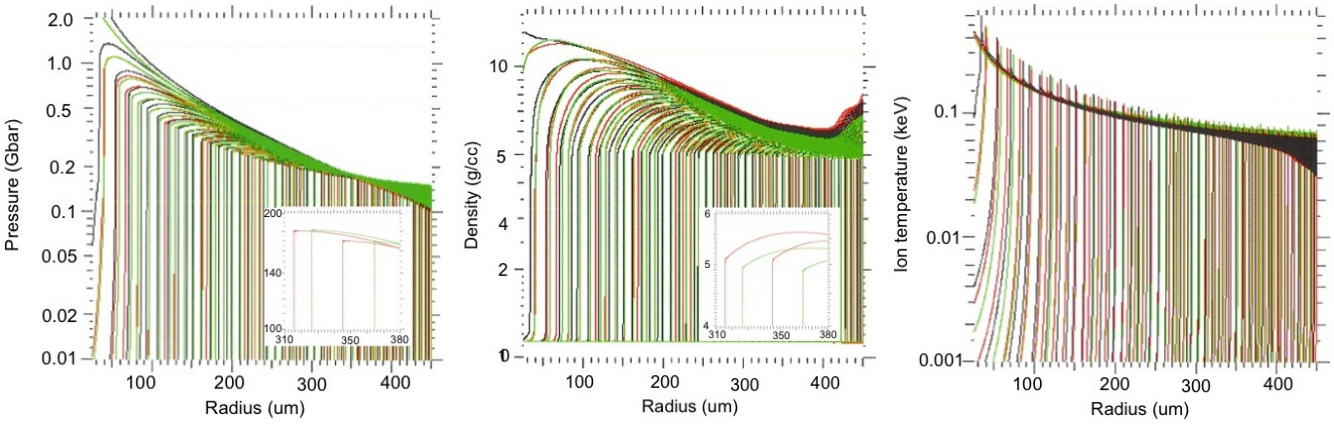

FIG. 5: Line-outs of the pressure, density, and ion temperature as a function of radius at various times for simulations using equation of state LEOS 5350 (red), LEOS 5400 (green), and Sesame 7592 (black). All choices of EOS show similar pressure, density, and temperature profile shapes.

torically modeled in a post-shot method for fitting to the experimental data [36].

In this work we start from a radiation drive, derived from experiment N111215, that has been tuned in this post-shot manner to match experimental observables in ICF implosions for a similar Hohlraum geometry, such as shock timing, implosion velocity, and neutron bang time. This radiation drive was modified to account for the fact that we will use eight of the 192 drive beams for the backlighter drive. In addition, the radiation drive is adjusted to account for the fact that we will shoot with a laser energy of 1.3 MJ in the first experiments, compared to 1.45 MJ for shot N111215, which will be achieved by shortening the length of the main pulse. In future experiments we will increase the requested laser energy to achieve a higher radiation temperature in the Hohlraum, which will enable the probing of Gbar pressures at larger radii. The radiation transport is modeled using multi-group Sn radiation transport, with 75 radiation groups.

The radiation temperature as a function of time is plotted in Fig. 2. The radiation drive launches four shocks into the ablator, which coalesce inside of the solid ball target. The EOS measurement takes place after the four shocks have coalesced into one single strong shock. The shock trajectories are shown in Fig. 2 via the logarithmic radial derivative of the pressure, plotted verses time and Lagrangian radius.

The simulations have been performed with three choices of EOS: LEOS 5350 (GDP), LEOS 5400 (GDP), and Sesame 7592 (polystyrene). Sensitivities of key measurables to choice of EOS are investigated. Here, tabular OPAL opacities are used [37]. Figure 3 shows princi-

ple Hugoniot curves for polystyrene using LEOS 5350 and 5400, Sesame 7592. The red and green over-plotted points correspond to pressures and densities that are extracted from the rad-hydro simulations using the LEOS 5350 (red) and LEOS 5400 (green) equations of state, respectively. This shows that after shock coalescence the shock follows the principle hugoniot and preheat is not significant. Sensitivity of the equation of state to uncertainty in initial target density and initial temperature is shown in Fig. 3 for EOS LEOS 5350. If the preheat is < 1eV, the effect on EOS is not significant in the 100 Mbar-1Gbar pressure range. Uncertainties in the initial density of 5% results in significant variation of the shock Hugoniot, and will need to be much better constrained for the experiment.

Figure 5 shows line-outs of the pressure, density, and ion temperature as a function of radius at various times for simulations using equation of state LEOS 5350 (red), LEOS 5400 (green), and Sesame 7592 (black). All choices of EOS show similar pressure, density, and temperature profile shapes but the magnitude of the density at a given pressure varies between the models, see the over-plotted points on 3. Also, see the insets in Fig. 5 for examples of density curves for LEOS 5350 and 5400 at 170 and 180 Mbar. At these pressures the density is lower by 2-4% for LEOS 5400. Contour plots of the pressure, density, and ion temperature as a function of radius and time for simulations using equation of state LEOS 5350 are shown in Fig.4. The contour plot of ion temperature shows that the preheat from Au M-band absorption past the Ge preheat shield of <0.3 eV.

The pressure as a function of shock radius is shown in Fig.6, which is about the same for all choices of equation of state. For these drive conditions we predict to reach pressures of > 400 Mbar at sample sizes of 100μm and $>$ 700 Mbar at 50μm. Figure 6 shows shock front position as a function of time and a zoom-in at late-times. The bang time varies by 40-50 ps between each choice of EOS model: 25.25 ns for LEOS 5400, 25.29 ns for Sesame 7592, and 25.34 ns for LEOS 5350. At 22.0 ns, the shock speed for all choices of EOS is $\sim$120-125 km/s at a radius of 547μm for LEOS 5350, 544μm for Sesame 7592, and 541μm for LEOS 5400. At 25.0 ns, the shock speed and radius is 220 km/s and 106μm for LEOS 5350, 230 km/s and 98μm for Sesame 7592, and 240 km/s and 86μm for LEOS 5400.

The probing time for the streaked radiography will range from 21 ns after the start of the laser pulse (which is the time that the laser pulse turns off) to 26 ns. Due to current constraints on the spectrometer design, we are limited to one x-ray scattering probing time per shot [41]. The probing time for the x-ray scattering will either be at 24.5 ns (before the shock reaches the center) or 25.5 ns (after the shock has rebounded), 3.5-4.5 ns after the laser pulse turns off.

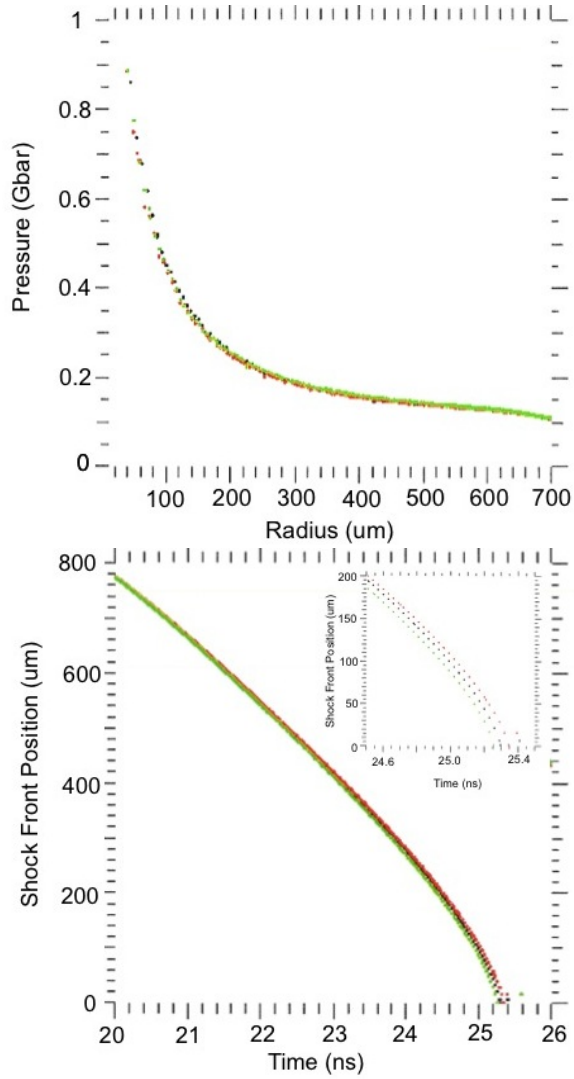

FIG. 6: (top) Pressure as a function of shock radius for simulations using equation of state LEOS 5350 (red), LEOS 5400 (green), and Sesame 7592 (black). (bottom) Shock front position as a function of time for simulations, with the inset showing more detail at late times. The bang time varies by 40-50 ps between each choice of EOS model: 25.25 ns for LEOS 5400, 25.29 ns for Sesame 7592, and 25.34 ns for LEOS 5350.

X-RAY RADIOGRAPHY

Time-resolved x-ray radiography will be used to measure the shock speed u_s and mass density ρ of shocked material. For 1D time resolution and 1D imaging we will use an x-ray streak camera together with an imaging slit to record the radiographic measurement. This method of streaked radiography has been demonstrated at the NIF in the convergent ablator campaign, designed to measure the velocity and thickness of imploding capsules [14, 15]. Here we employ solid sphere targets to enable reaching

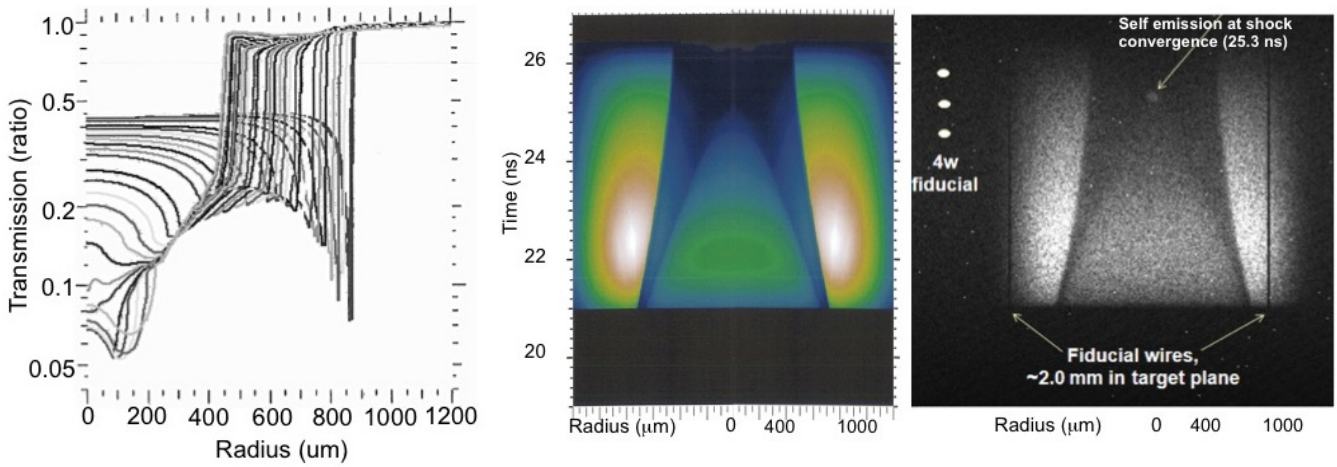

FIG. 7: (Right) Lineouts of x-ray transmission at 9 keV through the sample as a function of capsule radius for several times ranging from 16 to 27 ns. (center) Simulated radiograph of 9 keV x-rays through the sample as a function of time and capsule radius. Here, the integrated transmission is convoluted with the backlighted function in time and space. (Left) Simulated radiograph shown in the center with a noise function derived from previous shots. Also plotted is the location of the predicted self-emission flash, absolute values of the self emission are not show. Fiducial wires will be used to determine the magnification of the instrument and a 4ω fiducial will be used to determine the absolute diagnostic timing.

high pressures in a configuration that results in a less complicated EOS analysis.

In a steady shock, Rankine-Hugoniot relations use the conservation of momentum, mass, and energy transfer to the shock front to relate the pressure P and density $\rho = 1/\nu$ in the shocked state to the unshocked material (subscript 0), given u_s (Eqs. 1-3). Thus, by measuring ρ and u_s we constrain the thermodynamic variables across the shock front.

$$u_s^2 = \nu_0^2 \frac{P - P_0}{\nu_0 - \nu} \tag{1}$$

$$P = u_s^2 \rho_0 (1 - \rho_0/\rho) \tag{2}$$

The measured radiograph shows the position of the shock and the change in x-ray attenuation across the shock as a function of time, see Fig. 7 for a simulated radiograph and lineouts of the 9 keV transmission through the sample as a function of capsule radius. The density profile can be better constrained using a solid sample as the density of the unperturbed material inside of the shocked region is known. The shock speed is then determined from the locus of shock positions as a function of time. If the opacity of the sample at the x-ray energy is known, the density can be extracted from the attenuation at the shock.

To accurately constrain the EOS at the pressures and temperatures reached in these experiments, where the opacities are expected to deviate from cold opacities, we are in the process of developing a new analysis technique to extract the opacity and density simultaneously from the radiographic signal using the hydrodynamic flow equations. If the shock can be followed inward from the instant it first passes some identifiable radiographic marker, such as a layer of dopant or a change in composition (the sample/ablator interface), then the density profile outside the shock can be unfolded from the known part of the opacity profile, and both the density and opacity can be determined for the increment of material traversed by the shock.

X-RAY THOMSON SCATTERING

The shape and intensity of the scattered x-ray signal is related to the total structure factor of the plasma $S(\mathbf{k}, \omega)$ [38, 39] that describes the spectrum of electronic density correlations, or the Fourier transform of the probability of finding ions and electrons with respect to other ions and electrons in the plasma times σ_T, the Thomson scattering cross-section ($6.65\text{x}10^{-25}\text{cm}^{-2}$).

$$\frac{d^2\sigma_T}{d\Omega d\omega} = \sigma_T \frac{k_1}{k_0} S(\mathbf{k}, \omega) \tag{3}$$

Here, k_1 and k_0 are the scattered and incident radiation wave vectors, respectively. The total structure factor contains three main terms that result in observed features in the scattered photon spectrum

$$S(\mathbf{k}, \omega) = |f_I(k) + q(k)|^2 S_{ii}(k, \omega) + Z_f S^o_{ee}(k, \omega) + Z_c \int S_{ce}(k, \omega - \omega') S_s(k, \omega') d\omega' \tag{4}$$

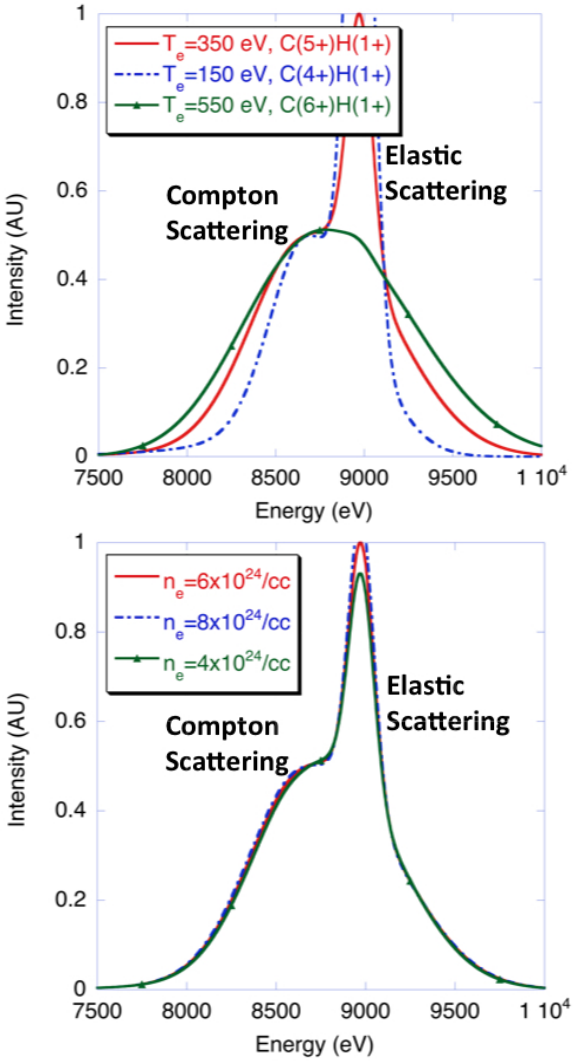

FIG. 8: (top) Synthetic x-ray scattering spectra of photons by indirectly driven solid CH samples probed at 25 ns for varying electron temperature and ionization at a fixed n_e=6x10^{24}/cc, showing the sensitivity of the Compton feature width to T_e. Here the Compton downshifted feature reflects the electron velocity distribution. (bottom) Synthetic x-ray scattering spectra for varying electron density at a fixed electron temperature of 350 eV. Here, the width of the Compton feature is insensitive to electron density.

where Z_f and Z_c are the effective free and core electronic states of the system. The first term in Eq. (4) results from the scattering of photons by tightly bound electrons that dynamically follow the ion motion, where $S_{ii}(k,\omega)$ is the ion-ion density correlation function, the ion-ion form factor, $f_I(k)$, accounts for scattering from core electrons, and $q(k)$ describes scattering from a screening cloud of free electrons surrounding the ions. The second term reflects the scattering of photons by free electrons that do not follow ion motion, where $S^o_{ee}(k,\omega)$ is the electron-electron density correlation function. The third term describes inelastic scattering due to bound-free transitions. Here, $S_s(k,\omega)$ represents a modulation due to the self-motion of the ions.

In the first experiments the non-collective behavior of the plasma will be probed, where the scattering parameter $\alpha_e = 1/k\lambda_S = hc/(E_0 2\pi\lambda_S) < 1$. Here, k is the magnitude of the x-ray scattering vector, where $k = (4\pi E_0/hc)\sin(\theta_s/2)$, and λ_S is the Debye or Thomas-Fermi screening length. The scattering regime can be set by choosing the energy of the probe x-rays, E_0, and the angle of the detected scattered x-rays, θ_s. For the conditions in this experiment and the calculated screening length, E_0=9 keV and θ_S=100°, the scattering parameter α_e ~0.25. In the non-collective (backscattering) regime, scattering from free electrons (second term in Eq. 4) results in a Compton scattering feature, downshifted in energy, that provides information on the electron velocity distribution through Doppler broadening. If the plasma is non-degenerate, probing the velocity distribution provides a measure of the electron temperature.

Figure 8 shows synthetic x-ray scattering spectra from the indirectly driven solid CH spheres with a Ge doped CH ablator at t=25 ns. Shown are the elastic and inelastic Compton scattering features at ~ 9 keV and ~8.82 keV, respectively. The Compton feature is down-shifted by the Compton energy, $\Delta E_C \sim 180eV$, and spectrally broadened by the electron velocity distribution due to Doppler shifting in the field of view of the detector. The simulated spectra listed on the top of Fig. 8 show the sensitivity of the Compton width to electron temperature. Here, the electron density was held constant at 6x10^{24}/cc and the electron temperature was varied. The ionization state was also corrected for self-consistency. However, calculations where the temperature was varied but the ionization state was held constant also resulted the same width variation in the Compton feature as a function of electron temperature. The simulated scattering spectra shown on the bottom of Fig. 8 show insensitivity in the Compton width to the Fermi temperature, and thus electron density. Here, the electron temperature was held constant at 350 eV and the electron density was varied. In these experiments, as predicted using radiation hydrodynamic simulations, the Fermi temperature, 120 eV, is lower than the predicted electron temperature, ~ 350 eV, resulting in a non-degenerate electron velocity distribution. Thus, the free-free x-ray scattering probes a Maxwell-Boltzmann distribution in the plasma, providing information on the electron temperature through the width of the Compton feature.

In the first experiments we estimate to detect 4x10^3 scattered photons, which is on the order of the number detected in previous Omega experiments, see Fig. **??** for an example of scattering from spherically imploding CH shells, see [18] for additional information on the experimental setup. Measurements at the NIF of the Zn backlighter probe with the pulse shape shown in Fig.1 b) have demonstrated conversion efficiencies for creating Zn He-

α x-rays from incident backlighter energy of up to one percent. Then, for a total backlighter energy of 40 kJ, and over an integration time of 200 ps, we will produce about 2.3x10^{16} backlighter photons. For a source to target solid angle of about 5x10^{-5}, this results in 1x10^{12} photons at the scattering target. Then, for an electron density of 6x10^{24}/cc, Thomson scattering cross section of 6.65x10^{-25}cm^2, and sample diameter probed of $\sim$ 300 μm, we will scatter about 1.3x10^{11} photons. For a target transmission of about 10%, a filter transmission of 60%, and a crystal solid angle of 3x10^{-5} (due to the finite size of the crystal and a HOPG reflectivity of $\sim$3 mrad [40]), 8x10^4 photons are reflected onto the image plane of the x-ray framing camera. For a quantum efficiency of 5%, about 4x10^3 photons will be detected.

A cylindrically bent HOPG crystal will be used in the first experiments to provide adequate spatial resolution for resolving the Compton down-scattered feature. Also, the HOPG lattice spacing, that determines the crystal geometry for a given back-lighter energy, satisfies the NIF beam interference requirements for operation in the polar DIM on a full system shot with nominal NIC ignition pointing. In these experiments we are limited by the strength of the x-ray probe that prohibits the use of heavy collimation to achieve high spatial resolution. Therefore, the scattered spectrum will reflect the electron density weighted electron temperature. To achieve higher spatial resolution in future experiments, additional probe beams and collimation can be employed. In addition, we will investigate the use of focusing LiF crystals, as opposed to HOPG crystals, that will provide higher spatial resolution in the non-dispersive direction, while achieving a comparable integrated reflectivity of the scattered photons.

CONCLUSIONS

In summary we have developed an experimental platform to probe the plasma conditions of matter at Gbar pressures at the NIF using x-ray radiography and x-ray Thomson scattering. Using x-ray radiography we will measure the shock speed and x-ray transmission and infer the opacity and mass density profiles of indirectly-driven, single-shock compressed solid CH, CD, or HDC spheres. The pressure will be determined using the Rankine-Hugoniot relations, thereby constraining the equation of state of the target material. X-ray scattering will be employed to measure the electron temperature of the shocked material and infer an ionization state through measurement of the bound-free scattering. These experiments have been accepted for NIF shot time in FY12-FY15 under the NIF basic science allocation. These experiments will provide accurate measurements of the equation of state and opacity under conditions important for the study of giant exoplanets and star formation.

ACKNOWLEDGMENTS

This work was performed under the auspices of the U.S. Department of Energy by Lawrence Livermore National Laboratory under Contract No. DE-AC52-07NA27344 and supported by Laboratory Directed Research and Development Grant No. 11-ER-050. RWF acknowledges support from SSAA program Contract No.DE-FG52-06NA26212.

[1] L. Stixrude, Phys. Rev. Lett. **108**, 055505 (2012).
[2] S. Seager *et al.*, Astrophys. J. **669**, 1279 (2007).
[3] V. Fortov, Extreme States of Matter: On Earth and in the Cosmos, 224 (2011).
[4] J. C. Pain, High En. Den. Phys., **3** 204 (2007).
[5] E. I. Moses *et al.*, Phys. Plasmas **16**, 041006 (2009).
[6] J. Nuckolls *et al.*, Nature, **239** (1972).
[7] J. D. Lindl *et al.*, Phys. Plasmas **11**, 339. (2004).
[8] R. Cauble *et al.*, Phys. Rev. Lett. 80, 12481251 (1998).
[9] N. Ozaki *et al.*, Phys. Plasmas, 12 (12), 2005.
[10] M. A. Barrios *et al.*, Phys. Plasmas 17, 056307 (2010).
[11] Phys. Plasmas, 12(8), 082702, 2005.
[12] T. R. Boehly, AIP Conf. Proc. 955, pp. 19-22 (2007).
[13] N. Ozaki *et al.*, Phys. Plasmas, 16 (6), 2009.
[14] D. G. Hicks *et al.*, Rev. Sci. Instrum. **81**, 10E304 (2010).
[15] D. G. Hicks *et al.*, Phys. Plasmas 19, 122702 (2012)
[16] D. C. Swift *et al.*, LLNL Report No. LLNL-PROC-492261, (2011).
[17] S. H. Glenzer *et al.*, Rev. Mod. Phys. **81**, 1625 (2009).
[18] A. L. Kritcher *et al.*, Phys. Rev. Lett. **107**, 015002 (2011).
[19] A. L. Kritcher *et al.*, Science, **322**, 69 (2008).
[20] L. B. Fletcher *et al.*, Phys. Plasmas 20, 056316 (2013)
[21] G. Gregori *et al.*, Phys. Rev. Lett. **101**, 045003 (2008).
[22] H. J. Lee *et al.*, Phys. Rev. Lett. **102**, 115001 (2009).
[23] B. Barbrel *et al.*, Phys. Rev. Lett. **102**, 165004 (2009).
[24] D. Riley *et al.*, Phys. Rev. Lett. **84**, 8 (2000).
[25] S. W. Haan *et al.*, Nucl. Fusion **44**, S171 (2004).
[26] J. L. Kline *et al.*, Phys. Rev. Lett. **106**, 085003 (2011).
[27] S. H. Glenzer *et al.*, Phys. Rev. Lett. **106**, 085004 (2011).
[28] S. H. Glenzer *et al.*, Science **327**, 1228 (2010).
[29] E. L. Dewald *et al.*, Rev. Sci. Instrum. **81**, 10D938 (2010).
[30] P. Michel *et al.*, Phys. Rev. Lett. **102**, 025004 (2009).
[31] N. B. Meezan *et al.*, Phys. Plasmas **17**, 056304 (2010).
[32] G. A. Kyrala *et al.*, Rev. Sci. Instrum. **81**, 10E316 (2010).
[33] D. H. Kalantar *et al.*, Rev. Sci. Instrum. **72**, 751 (2001).
[34] J. A. Oertel *et al.*, Rev. Sci. Instrum. **77**, 10E308 (2006).
[35] M. Marinak *et al.*, Phys. Plasmas **5**, 1125 (1998).
[36] D. S. Clark *et al.*, Phys. Plasmas 20, 056318 (2013)
[37] C. A. Iglesias and F. J. Rogers, Astrophys. J. 464, 943 (1996).
[38] J. Chihara, J. Phys. F: Met. Phys. **17**, 295 (1987).
[39] J. Chihara, J. Phys. : Condens. Matter **12**, 231 (2000).
[40] A. Pak *et al.*, Rev. Sci. Instrum. **75**, 10 (2004).
[41] T. Döppner *et al.*, *Publication in progress.*